DOI 10.4430/bgo00404

Geophysical methods for investigating source rocks

V. De Tomasi and G. Gambacorta

Eni S.p.A. Natural Resources, San Donato Milanese, Italy

(Received: 5 April 2022; accepted: 6 September 2022; published online: 11 November 2022)

ABSTRACT The estimation of kerogen volume and quality in source rocks is fundamental for evaluating a basin's hydrocarbon potential. Methods for kerogen estimation are based upon chemical and mechanical analysis of rock samples from outcrops or cores, thus limiting the spatial accuracy of petroleum system models far from hard data. Recent works demonstrated the possibility of using acoustic impedance inversion and amplitude versus angle analysis from surface seismic data for qualitative and quantitative estimation of kerogen. These methods are discussed in detail, and practical applications to real data are presented. Since kerogen is a considerably anelastic material, a frequency-dependent seismic attribute (sweetness) was tested, and its sensitivity to kerogen presence was investigated. A method for impedance inversion without wells, based upon local impedance constraints is demonstrated as a tool to delineate the distribution of kerogen in undrilled areas. Comparison between rock physics models and rock core samples showed that source rock impedance depends not only on kerogen percentage but also on its origin, with marine algal kerogen showing a lower impedance than terrestrial kerogen. This adds ambiguity to the interpretation of results, which can be solved with help of *a priori* assumption from sedimentary information related to organofacies accumulation.

Key words: kerogen, source rock, impedance, seismic attributes.

1. Introduction

The identification and evaluation of source rocks is one of the first steps in estimating the hydrocarbon potential of a sedimentary basin. The amount and type of kerogen contained in source rocks determines the quality and quantity of available hydrocarbons, information that is key for determining the economic importance of a basin. The analysis of the kerogen present in a source rock is routinely done by collecting source rock samples either from outcrops or from well cores. The samples are then analysed with chemical and physical methods to determine kerogen type, amount and maturity. Unfortunately, the limited availability of physical samples restricts the degree of accuracy that can be reached when mapping kerogen vertical and lateral distribution.

Previous examples have demonstrated the possibility of using surface seismic data for detecting kerogen in source rocks (Løseth *et al*., 2011). Viscoelastic properties of kerogen are quite different than those of surrounding rocks, so its presence causes seismic anomalies that can be observed with seismic surveys. Impedance inversion and amplitude versus angle (AVA) methods have been proposed as tools for investigating kerogen abundance in source rocks. Models have been computed describing wave propagation in kerogen rich rocks (Carcione, 2000), and templates for analysing the reflections have thus been published.

A research and test program to evaluate and possibly improve seismic methods for total organic carbon (*TOC*) content estimation was started by our group. Our tests were mostly performed on data coming from an area in Tunisia, in the northern part of the Ghadames Basin. In this area, the Tanezzuft Formation (Silurian) represents a world-class source rock (Gambacorta *et al*., 2016; Amato del Monte *et al*., 2018), characterised by organic-rich facies with locally very high measured *TOC* content. Fig. 1 shows a map of the study area, together with the location of the four wells whose logs and core samples were considered in this work. Wells 1 and 4 are proximal, while wells 2 and 3 are relatively more distal.

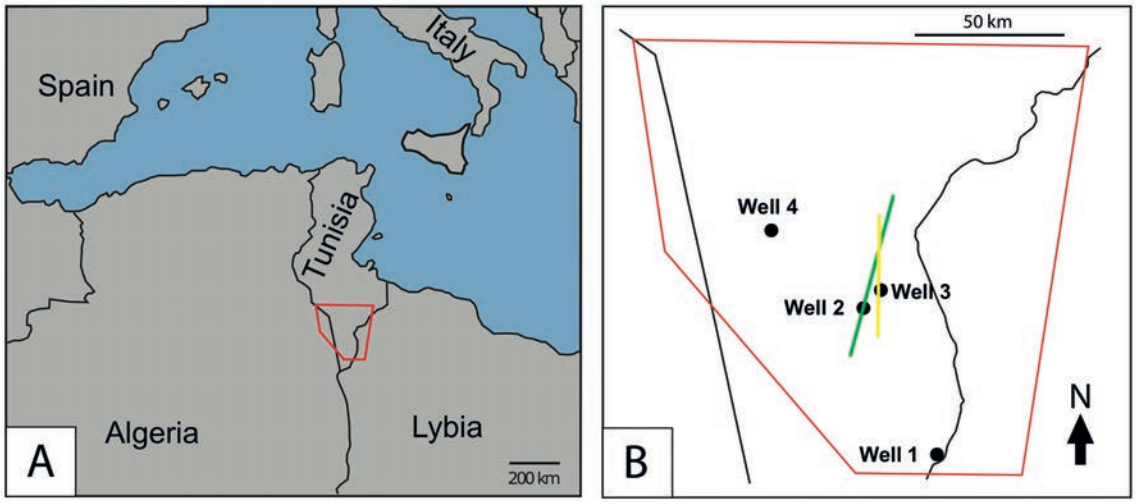

Fig. 1 - A: Location of the study area for the Tanezzuft Fm. B: Spatial distribution of wells in the area of interest (modified after Amato del Monte *et al*., 2016). The green line shows the profile of the 2D line used in the AI test, while the yellow line is the profile of the seismic line extracted from the 3D volume for AVA inversion.

Tanezzuft Formation (hereafter Fm.) is the most important source rock present in the Ghadames Basin (Tunisia). The source rock interval can be divided into two main parts: an upper part that can reach a thickness of about 50 m, known as 'warm shale' that is slightly enriched in organic matter with *TOC* on average lower than 2%, and a lower part known as 'hot shale' about 30 m thick, with *TOC* values that can reach up to 20%. The Silurian Tanezzuft Fm. lies over the Upper Ordovician glacial deposits of the Djeffara Fm. and is overlain by the Upper Silurian regressive marine sandstones of the Acacus Fm. As Tanezzuft Fm. does not outcrop in the study area, its direct characterisation can be performed exclusively based on available well data, thus limiting its mapping in areas poorly or not covered by wells. Many core samples were available from the Tanezzuft Fm., so that core lab measurements could be compared against rock physics model predictions. A 2D line and a small 3D survey were available, both crossing, or close to, some wells drilled through the source rock interval. This gave the opportunity to compare seismic predictions against well logs, and directly evaluate the capability of the techniques to detect kerogen. Despite the large availability of data covering the source rock interval, the quality of seismic data in this basin was unfortunately not always good, because of the poor seismic response of the area, source coupling problems and limited bandwidth. Tests were done on acoustic impedance (AI) inversion, AVA methods, and frequency-dependent seismic attributes (sweetness). As will be discussed, one of the inversion methods tested (Walker and Ulrych, 1983)

had problems with the quality of available data, then, seismic data from other basins were used to complete the tests, namely a line from North Sea and other data from basins in west Africa.

2. Theory and methods

2.1. Rock physics model

A rock physics model is helpful to determine the seismic response of a source rock formation and evaluate the detection possibilities with geophysical methods. Laboratory measurements on source rock samples can determine the amount of kerogen content and its type (that are controlled by the predominance of marine versus terrestrial organic matter - algal/sapropelic, planktonic, humic - and by its degree of maturity), as well as the type and abundance of accompanying minerals. Samples are usually taken from cores, sidewall cores, well cuttings or outcrops, even if their amount is severely limited in number due to the high costs involved in rock sampling and laboratory analysis.

A log curve describing the amount of kerogen present in the formations allows increasing the quantity of information available for modelling the vertical distribution of organic matter content. No log tool capable of directly detecting kerogen currently exists, but a method to derive a continuous *TOC* log curve from existing log data was proposed by Passey *et al*. (1990). This method is known in the literature as '*Δ*logR', and it uses the fact that kerogen presence causes both a significant increase of P-wave transit time *Δ* and a resistivity change. By combining the resistivity *R* and *Δ* transit time log curves, a regression function predicting *TOC* can be computed as follows:

$$TOC = m\Delta log(R) - q \tag{1}$$

where *Δ* is the P wave sonic transit time, *R* the formation resistivity, and *m*, *q* are coefficients determined by fitting Eq. 1 to the *TOC* values obtained from the available core samples. Sometimes the sonic log is not reliable, due to the low velocity of kerogen-rich formations, so it can be advantageous to rewrite Eq. 1 using Gardner's relationship (Gardner *et al*., 1974) between the formation density *ρ* and V_P:

$$\rho = aV_P{}^b = a\left(\frac{K}{\Delta}\right)^b \tag{2}$$

where *K* is the conversion factor between the reciprocal of the slowness log curve and sonic wave velocity, and *a* and *b* are Gardner's coefficients, and combining Eqs. 1 and 2:

$$TOC = \frac{mKlog(R)}{\sqrt[b]{\frac{\rho}{a}}} - q \tag{3}$$

The *TOC* log curve generates an accurate model of the vertical kerogen distribution in a basin, nevertheless, the model so obtained is very coarse especially in the first stage of evaluation of the basin hydrocarbon potential, when very few wells have been drilled and there is little

understanding of the lateral variability of kerogen distribution.

It has been shown that seismic data can be used to map *TOC* distribution (Løseth *et al*., 2011), but to associate properties estimated from seismic data (reflectivity, impedance, etc.) with the *TOC* percentage, a rock physics model describing the (visco)elastic behaviour of the source rock is needed. The physical distribution of organic matter within a black shale can be very schematically grouped into two major classes, laminated or dispersed, depending on the way organic matter production, preservation and dilution controlled the sedimentation of the organic fraction. Laminated rocks can be modelled using the Backus model, resulting in an anisotropic equivalent solid, while dispersed ones are best modelled using Voigt averaging (Mavko *et al*., 2003). In this work, only laminated shales will be considered, since they represent the most common finding in black shales.

Calculating Backus model also requires knowing the elastic moduli of kerogen, but very few data are available in literature. Carcione (2000) reported some kerogen moduli used in the calculations described in his works, but the related literature from where these data were reported could not be traced back. Yan and Han (2013), instead, reported the results of laboratory measurements obtained after rock dissolution, kerogen separation, and pelletisation. The two values are very different from each other, and no details about kerogen origin and degree of maturity could be obtained from the two papers. Both data sets were used for calculating Backus model and, as will be shown later, surprisingly they both are pertinent to the area we studied, when compared against data samples distribution.

2.2. Impedance inversion

Measuring AI with seismic inversion has been proposed as a method for detecting kerogen presence in source rocks (Løseth *et al*., 2011). In practice, inversion can show kerogen-rich layers as low impedance anomalies, contrasting significantly against the impedance of the surrounding rocks. The AI versus *TOC* relationship calculated from a rock physics model can be used to transform the impedance seismic image into the *TOC* one. However, it will be shown that this relationship is not unique, and this sets some limits on the use of the method.

Impedance inversion requires the availability of a low frequency impedance model, which is usually obtained by combining the seismic velocity field with AI logs acquired from sonic and bulk density log curves. This is because seismic data cannot record low frequencies, and these frequencies are fundamental to determine the time trend of the inverted impedance. Model based inversion is routinely performed for reservoir characterisation: the fact that impedance can detect the presence of kerogen makes acoustic inversion a tool of interest for basin evaluation. Unfortunately, the need for well log data to construct the model limits the application of inversion to those basins where at least a well has been drilled.

To circumvent this limitation, a near-forgotten inversion algorithm by Walker and Ulrych (1983) was considered. The algorithm replaces the low frequency impedance model with some constraints defined either as $AI(t) = AI_0$ or $AI_1 < AI(t) < AI_2$ (Ulrych and Walker, 1984), where AI_0, AI_1 and AI_2 are prescribed constraining values for impedance at time t. The constraints vary laterally and need to be estimated to assure inversion stability. The missing frequencies are reconstructed with a clever scheme, where first an autoregressive (AR) operator is calculated to approximate the known frequency spectrum, and, then, the missing low frequency spectrum is interpolated so that it respects both the AR operator prediction and the impedance constraints. More details can be found in Walker and Ulrych (1983): the original algorithm was tested, but the suggested L1/L2 optimisation algorithm by Barrodale and Roberts (1980) was replaced in our implementation

with Shor's method (Kappel and Kuntsevich, 2000). The optimisation problem is formulated in the Huber's norm (Guitton and Symes, 2003), but, instead of using their solution method, the Kappel and Kuntsevich *solvopt* algorithm is used, that implements an exact penalisation method [see discussion in Luenberger and Ye (2016)]. The *solvopt* starting point is chosen as the constrained L2 solution of the problem.

Impedance constraints need to be properly defined for this inversion method to work. It is generally easier to define inequality constraints, since exact values of the impedance of a layer are rarely known. The seismic interval velocities together with Gardner *et al*. (1974) law were used to define impedance boundaries. By multiplying the two sides of Eq. 2 by the P wave velocity V_p one obtains:

$$AI = a(V_P)^{1+b} \tag{4}$$

where *a* and *b* are Gardner's coefficients. So, one simply extracts the interval velocity along a horizon, and, then, converts the velocity into AI constraints with Eq. 4.

The work by Gardner *et al*. (1974) showed that the two parameters *a* and *b* are different for sand and shales, so the lower impedance boundary is set by estimating the lowest expected impedance for a sand at the given space-time position, and the upper boundaries is set to the shale impedance. The parameters presented in Gardner's paper were calculated for the Gulf of Mexico area: different basins need a recalibration of fitting parameters, otherwise large errors could result (Bai, 2016). For the method to work, the accuracy of AR operator in reconstructing the missing spectrum is crucial: it was found that if there are too few spectral samples the reconstruction becomes unstable, showing little continuity of the reconstructed impedance from trace to trace. If, instead, the reflectivity spectrum is wide enough and/or the signal to noise ratio (SNR) is favourable, the constrain-driven inversion gives results like model-driven inversion methods. No lateral continuity conditions were inserted in the implementation used for this work: a simple lateral median filter was used to pre-process seismic traces to improve lateral continuity.

2.3. Amplitude versus Angle

Rock properties like AI and Poisson ratio can be inferred by matching the theoretical AVA response, either using the exact (Aki and Richards, 1980) or approximate (Shuey, 1985) equations to the reflection amplitudes observed in pre-stack seismic data. Source rocks are often VTI (vertical transverse isotropy*)* anisotropic, and their anisotropy can significantly exceed the 'small anisotropy' approximation (Thomsen, 1986). Furthermore, kerogen has a very low Q factor with respect to rock minerals (Zezotarsky *et al*., 2004). Anelastic attenuation not only affects the seismic signal spectrum, but also affects reflection coefficients (Bourbié, 1982), and this can give some surprising and misleading results (Lines *et al*., 2014). So, certain care should be used in interpreting AVA results on source rocks with high *TOC*. Rüger (1997) three term approximation could be used to model anisotropy for AVA inversion:

$$R_P(\theta) = \frac{\Delta Z}{2\overline{Z}} + \left[\frac{\Delta V_{P0}}{\overline{V_{P0}}} - \left(\frac{2\overline{V_{S0}}}{\overline{V_{P0}}}\right)^2 \frac{\Delta G}{\overline{G}} + \Delta\delta\right]\frac{sin^2\theta}{2} + \left(\frac{\Delta V_{P0}}{\overline{V_{P0}}} + \Delta\epsilon\right)\frac{sin^2\theta}{2} tan^2\theta \tag{5}$$

where *Z* is the P impedance, *G* the S impedance, both determined along the vertical symmetry

axis, and δ and ε are Thomsen's small anisotropy parameters. Δ and the bar symbols are defined so that, if for example Z_1 and Z_2 are respectively the P impedances of the lower and upper layer, then $\Delta Z = Z_1 - Z_2$ and $\overline{Z} = (Z_1 + Z_2)/2$. Just like Thomsen's approximation, Rüger's one is valid for small values of δ, ε.

2.4. Seismic attributes

Since kerogen is an anelastic material (Zezotarsky *et al*., 2004), this can be exploited to detect kerogen presence, by measuring either the attenuation coefficient or the Q factor of the formation. Estimating the Q factor from surface seismic data is not easy, because of noise, local changes in seismic source spectrum, and its coupling to the surface lack of source emission at high frequencies, and so on. The use of a frequency-dependent seismic attribute, as a proxy indicator of anelastic attenuation, was then considered. Frequency dependent attributes are based upon the measurement of the instantaneous frequency that is defined as:

$$F(t) = \frac{1}{2\pi}\frac{d\Phi(t)}{dt} \tag{6a}$$

$$\Phi(t) = atan\left[\frac{y(t)}{x(t)}\right] \tag{6b}$$

where $x(t) + iy(t)$ is the complex seismic trace (Taner *et al*., 1979), Φ is the instantaneous phase, and F is the instantaneous frequency. Unfortunately, the instantaneous frequency attribute is unstable, since it depends on a ratio between two noisy quantities (Eq. 6b) and there is a time derivative in its definition (Eq. 6a), that causes an increase in noise content. Fomel (2007) proposed improving the frequency attribute by using Tikhonov regularisation, but his method, although functional, showed a limited vertical resolution. De Tomasi (2016) improved the method by using a different regularisation operator, obtaining a further noise reduction and an attribute vertical resolution close to the seismic resolution. The instantaneous frequency attribute by itself is not very useful for detecting kerogen-rich source rocks, since the attribute oscillates notably when thin layers are present. However, it is possible to combine the frequency attribute with others, namely the instantaneous amplitude, to obtain derived attributes that are sensitive to both frequency and amplitude variations. We tested the sweetness attribute $S(t)$ (Radovich and Oliveros, 1998), which is defined as:

$$S(t) = \frac{A(t)}{\sqrt{F(t)}} \tag{7}$$

where the instantaneous amplitude $A(t)$ is represented by:

$$A(t) = \sqrt{x(t)^2 + y(t)^2} \tag{8}$$

where again $x(t)$ and $y(t)$ are the real and imaginary parts of the seismic complex trace. The sweetness attribute has found applications for GPR signal interpretation (Abdulrazzaq *et al*., 2021), but it is not often used in seismic interpretation. Since kerogen-rich source rocks cause

both strong reflections and an anelastic attenuation anomaly, their reflections should be characterised by a sweetness anomaly. Unfortunately, there are no models that can predict the sweetness value associated with a corresponding *TOC* value, unless attribute calibration is done with the help of a well log or a *TOC*-calibrated seismic impedance line. Furthermore, lateral variations of the overburden anelastic attenuation or of the source emission can significantly perturb the sweetness attribute. Therefore, the sweetness attribute should be considered, at the current state, just as a qualitative indicator of the presence of kerogen.

3. Results and discussion

3.1. Rock physics model

A significant amount of core samples was available for source rock characterisation. Standard laboratory measurements (X-ray fluorescence XRF, kerogen analysis, acoustic transit time, etc.) were performed on samples, and $\Delta \log R$ log curves were calculated from well logs. By grouping and averaging the compositions of core samples, we defined average compositions of the Tanezzuft source rock interval and of the formations located below (Djeffara Fm.) and above (Acacus Fm.) the studied source rock interval. Averaged composition has been summarised in Table 1, together with the results of the Backus calculation. Mineral properties for the calculation were obtained from the works by Carcione (2000) and Yan and Han (2013). We calculated two different Backus models, one using Carcione's data for kerogen, and another from Yan and Han's work: the calculations were done by keeping constant the volume occupied by kerogen, illite, and smectite, and keeping the smectite/illite ratio equal to 1, as determined by averaging core samples data. The concentration of pyrite was kept fixed at 8.9%, and that of quartz at 25.1%.

Table 1 - Elastic properties of the components of the source rock model used in our study. Kerogen 1 refers to the data published by Yan and Han (2013), Kerogen 2 refers to Carcione (2000).

	V_{11} (km/s)	V_{33} (km/s)	V_{55} (km/s)	V_{66} (km/s)	V_{12} (km/s)	ρ (g/cm^3)
Smectite	3.86	3.14	1.53	2.14	2.15	2.3
Illite	4.70	4.36	2.46	2.77	2.43	2.7
Quartz	6.03	6.03	4.12	4.12	1.56	2.65
Pyrite	8.11	8.11	5.18	5.18	3.46	4.93
Kerogen 1	1.90	1.90	0.60	0.60	1.97	1.20
Kerogen 2	2.60	2.60	1.20	1.20	1.97	1.40

In Fig. 2 the calculated curves of AI versus *TOC* value are shown: the model calculated with Carcione's kerogen values is indicated by a red line, while Yan and Han's model is drawn with a black line. The large discrepancy between the two models for increasing *TOC* values is evident. Data points of core samples from four wells were used to compare model prediction with lab measurements. Data points from Well 2 closely follow the predicted AI-*TOC* curve calculated with Yan and Han's model, while the data from the other wells are scattered between the two model lines. Well 2 is in a relatively distal environment away from the paleo-coastline, so the kerogen present in the source rock at this location is mainly dominated by marine organic matter. Also Well 3 is relatively distal, but it is located closer to the coastline than Well 2. Its data points

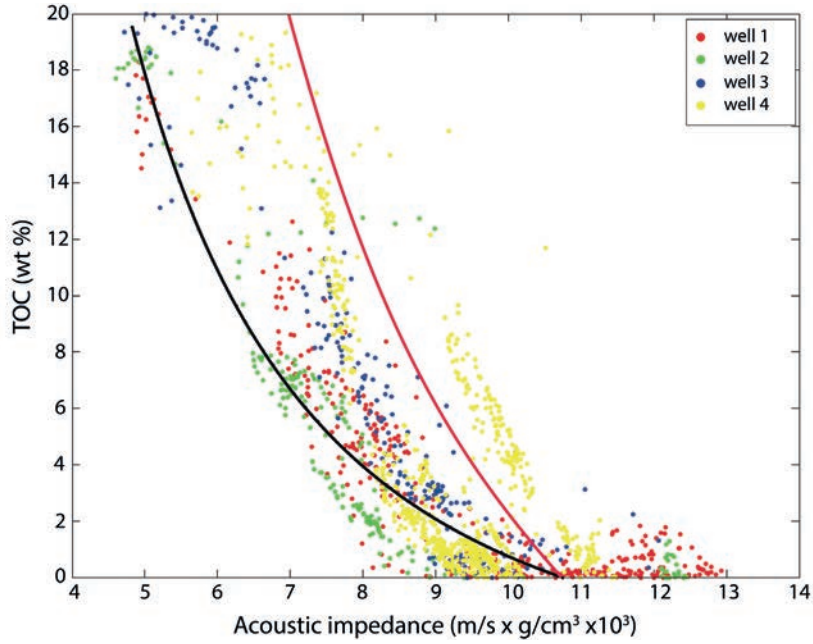

Fig. 2 - Distribution of *TOC* - impedance pairs. The black line is the response predicted by the Backus model with Yan and Han (2013) kerogen parameters, while the red line represents the response using those proposed by Carcione (2000). See text for details.

are somehow scattered between the two model lines, thus suggesting a mixed contribution from both marine and terrestrial organic matter. Wells 1 and 4 are the most proximal with kerogen at these locations mainly of terrestrial origin.

The data published by Yan and Han (2013) and Carcione (2000), together with the data collected from core samples at the four well locations suggest that elastic moduli of kerogen depend on its origin, with terrestrial kerogen being the stiffer one. Unfortunately, very little data have been published showing a complete characterisation of kerogen in terms of elastic moduli, anelastic attenuation, kerogen origin, and maturity, so it is difficult to analyse the data further.

From model calculations and experimental data, we observed that the association of AI with *TOC* value is ambiguous, and knowledge of the sedimentation model is needed to remove the ambiguity. In fact, as shown in Fig. 2, a very low value of impedance can be associated with a large *TOC* value of marine algal origin, just as very high impedance values can be interpreted as linked to organic-lean intervals. On the other side, 'intermediate' impedance values can either be the consequence of the presence of a large amount of terrestrial kerogen, a small amount of marine algal kerogen, or something in between.

When studying the *TOC* distribution, both in different source rocks and in the same source rock in different areas, we noticed variable trends in its relation with AI. In particular, in the data we studied we observed that distinct trends reflect the different amounts in marine versus terrestrial kerogen. We speculate that the stiffer nature of terrestrial organic matter compared to marine organic matter results in higher AI values for the same *TOC* content. In Fig. 3 we present an example of a *TOC* versus impedance data from a well in west Africa crossing different source rock intervals of different origin. The plot presents a 'double-tailed' trend that reflects the different elastic properties of associated to kerogens of different origin.

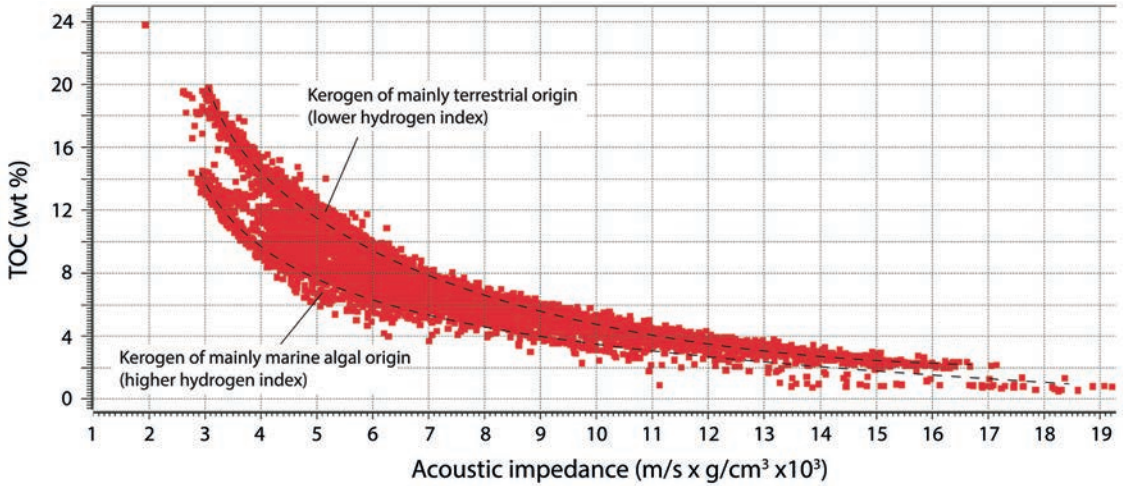

Fig. 3 - 'Two-tailed' distribution in *TOC*-AI scatter plot based on data coming from a basin in west Africa. Two different trends can be observed: one related to a softer (marine) kerogen, and another associated to a stiffer (mainly terrestrial) kerogen. See text for details.

3.2. Impedance inversion

Model-based inversion was calculated on a 2D post-stack seismic line covering mostly the distal part of the Ghadames Basin. The line crossed Well 2, so the Yan and Han (2013) kerogen model was selected as the most appropriate to transform AI into *TOC* values. Seismic data quality was poor, due to the limited seismic bandwidth (10-60 Hz) and to the low SNR. Only the post stack time image was available, so there was no opportunity to reprocess pre-stack seismic data to improve the stack quality. The low frequency model was estimated by fitting the filtered impedance log with the velocity field, and a commercial inversion software was used to calculate the AI. The result of inversion is shown in Fig. 4, while in Fig. 5 the impedance remapped into

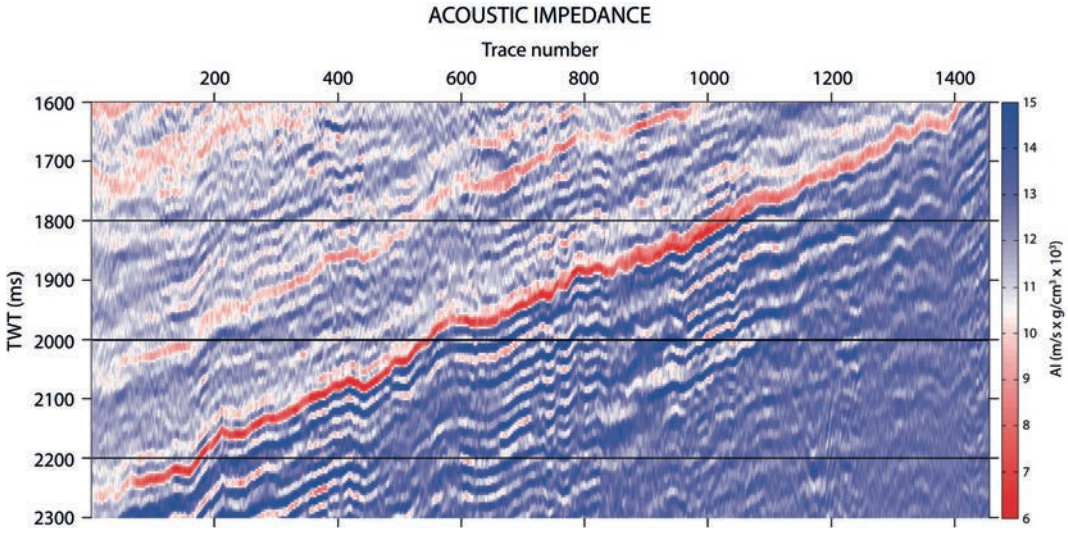

Fig. 4 - AI image of the Tanezzuft Fm. The source rock interval is the dipping red event located in the middle of the image.

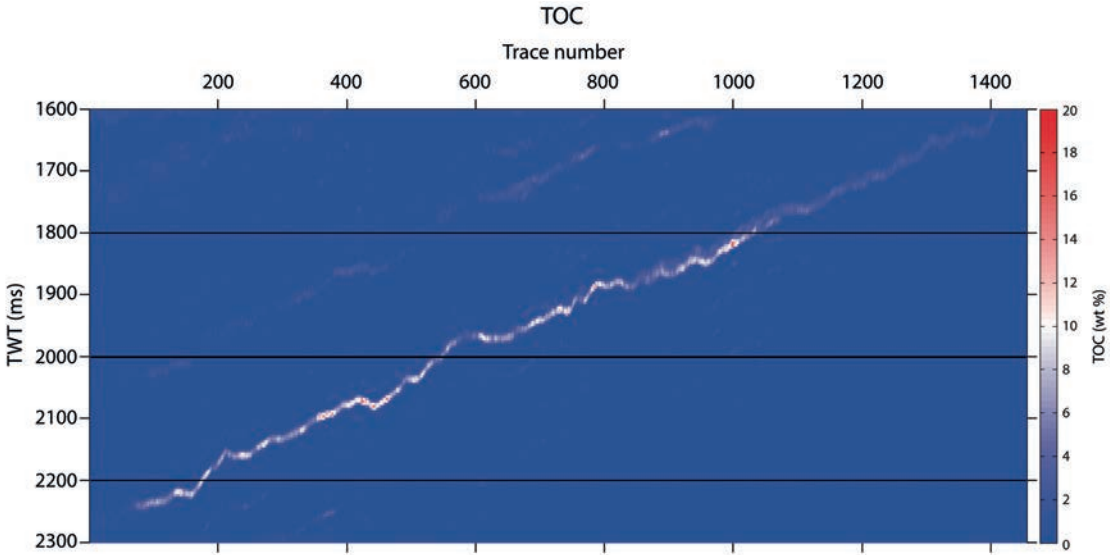

Fig. 5 - *TOC* image of the source rock. Kerogen properties by Yan and Han (2013) were used to convert AI into *TOC* values.

TOC values with the Yan and Han model is shown. Fig. 5 shows that *TOC* is unevenly distributed along the source rock interval, reaching concentrations up to 20% and maybe more in some locations. The amount of kerogen decreases moving away from the paleo-coastline towards the paleo-offshore along the north direction, as is expected from sedimentological and geochemical data (Gambacorta *et al*., 2016). The kerogen distribution shown by impedance inversion is quite different from the distribution one could obtain by mapping data from wells, since the kerogen spatial distribution is far from being uniform, and this has relevant consequences for the petroleum system modelling.

The Walker and Ulrych (1983) inversion was calculated on the same seismic line described before, but the results were unacceptable, showing plenty of artifacts and unrealistic impedance values. The main cause was due to the limited signal bandwidth and to the poor SNR. The algorithm requires the estimation of a robust AR operator in the frequency domain. When there are too few spectral data points to interpolate, the data are noisy, or the frequency gap to interpolate is too wide, the AR spectrum reconstruction becomes unreliable.

To compare the two inversion methods and assess the reliability of the Walker and Ulrych (1983) inversion, a test was done on a seismic line from the North Sea, for which a model-based inversion was readily available. The selected data set has a seismic bandwidth in the range 5-70 Hz, and, although the seismic response of the area was poor, the SNR was adequate. The velocity field was determined from tomographic inversion, but the deepest part of the model was found to be unreliable due to the reduced offset span of the survey, so inversion was limited to 2750 ms TWT. To calibrate Gardner's parameters for determining the impedance constraints for inversion, no data from wells close to the line location were used, but only some velocity-density data for the North Sea reported in the literature (Bai, 2016).

The results of the two inversion results are shown in Fig. 6 together with those obtained from the well-constrained inversion. As can be seen, the results are quite similar: the Walker and Ulrych (1983) inversion has some lateral artifacts mostly caused by lateral noise (probably residual time-migration artifacts) that was not properly removed during processing. There are

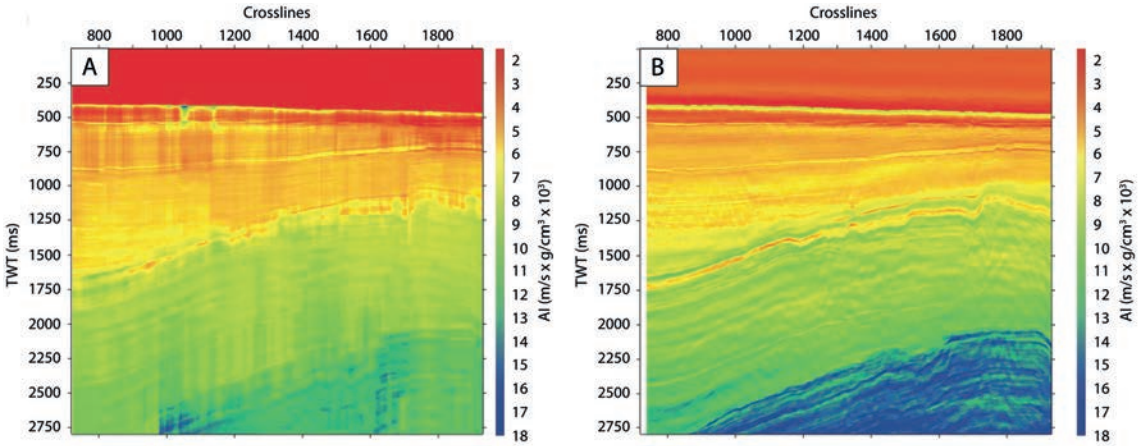

Fig. 6 - Comparison between A: AI inverted without wells and, B: with low frequencies recovered by combining well impedance with the velocity field.

visible differences in the deepest part of the image, with the model-based inversion showing unreliable values of AI, because of the velocity field extrapolation. The Walker and Ulrych inversion shows almost no extreme values of impedance there, because the deepest constraint was located right at the beginning of the extrapolated region.

The Walker and Ulrych inversion was then applied to a seismic line from a west Africa basin. In the region the source rock interval, although well-known from regional studies, could not be easily identified on the seismic image. The seismic bandwidth extended from 5 to about 80 Hz with a very good SNR. The velocity field came, as in the North Sea case, from a tomographic inversion. Constraints were calculated using Gardner *et al*. (1974) relationship tailored to the regional data. The seismic profile crossed an exploration well, but its log data were not used to calculate constraints, but only for checking their consistency against the impedance log.

The result of the inverted impedance is shown in Fig. 7. In the image, the two main reservoir intervals can be recognised, in particular the lowermost is marked by a black arrow, while the

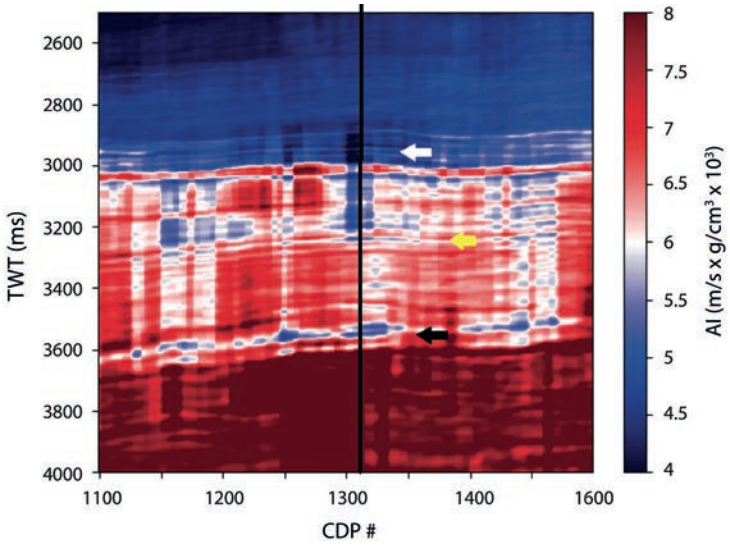

Fig. 7 - Result of impedance inversion without well. The vertical black line is the position of the well shown in Fig. 8. White and black arrows show the positions of the two reservoirs. The yellow arrow shows the position of the upper reservoir source rock.

uppermost reservoir is highlighted by a white arrow. A layer characterised by low AI, marked by a yellow arrow, is present between the two reservoirs at about 3250 ms TWT. This interval is characterised on a regional scale by a single loop event and generally highly reflective surfaces that tend to smoothly onlap towards the coastline. Based on available stratigraphy, this interval corresponds to marine shales with some sandstone characterised by an average *TOC* ranging from about 2 to 5 wt%. Organic matter is mainly marine with some contribution from continental organic matter, as supported also by hydrogen index values ranging on average from 300 to 400 mgHC/g*TOC*, thus indicative of a kerogen type II to II/III. The image is affected by some artifacts close to the well location, because the seismic line was shot after the well was drilled and the area began to be worked. The presence of the rig, pipelines, and other surface equipment caused coverage problems to the seismic data.

Fig. 8, finally, shows a comparison between the AI calculated from the well log and the impedance estimated with the Walker and Ulrych (1983) inversion close to the well position: the vertical segments show the constraints calculated from the velocity field. As can be seen, the match between log impedance, seismic inverted impedance and impedance constraints is satisfactory.

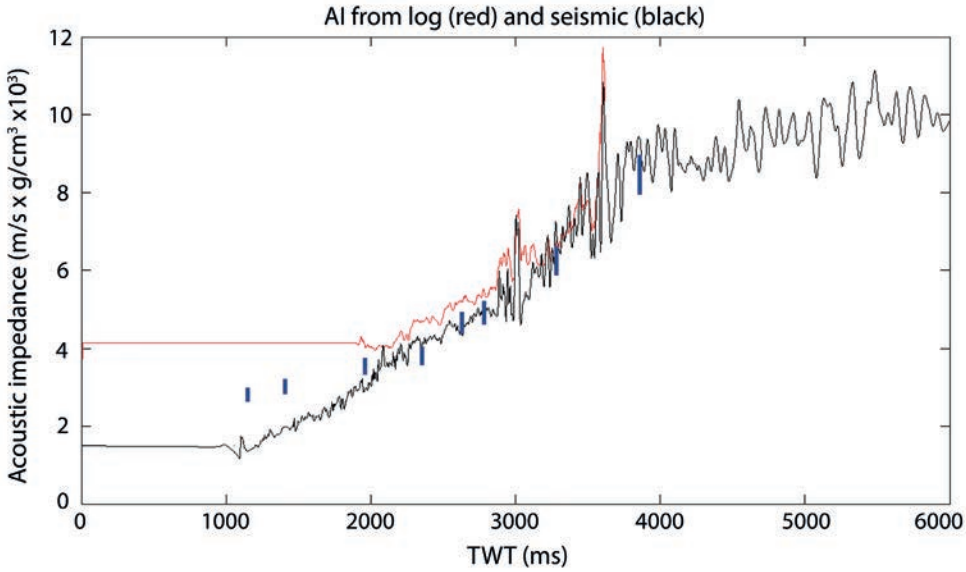

Fig. 8 - Comparison between AI from well log (red) and AI from inversion without wells (black) (Walker and Ulrych, 1983). The vertical blue segments show the impedance constraints used for controlling the inversion. Constraints have been calculated from the velocity field using Gardner's law. Blue bars are the constraints used for inversion: the first constraints were not fulfilled by inversion because of incorrect geometrical spreading correction of seismic data (the constraints are implemented in our inversion as 'soft' constraints).

3.3. Amplitude versus Angle

The AVA method was applied to a line from a small 3D survey located close to wells 2 and 3 in the Ghadames Basin. The expected AVA response was modelled by averaging the elastic parameters of the formation of interest from log data, and, then, fitting Rüger's (1997) equation 5 to the data to obtain the anisotropy parameters. The model parameters used for the warm

shale are V_P = 4056 m/s, V_S = 2019 m/s, ρ = 2.694 g/cm^3, ε = 0.30, and δ = −0.35 and for the hot shale V_P = 3302 m/s, V_S = 1812 m/s, ρ = 2.48 g/cm^3, ε = 0.70, and δ = −0.15, where ε and δ are Thomsen's small anisotropic parameters. The anisotropy parameter values exceed the small anisotropy assumption, probably because of the effects due to the high *TOC* value. The AVA model predicted for the warm/hot shale interface a class IV response. Reflections were extracted from the seismic line and plotted in the intercept/gradient plane. The data points have been colour-encoded with their position along the seismic line (Fig. 9). Due to the presence of kerogen, the AVA effect decreases when moving north far from the paleo-coastline, in accordance with what has been shown by the impedance inversion and with the depositional model.

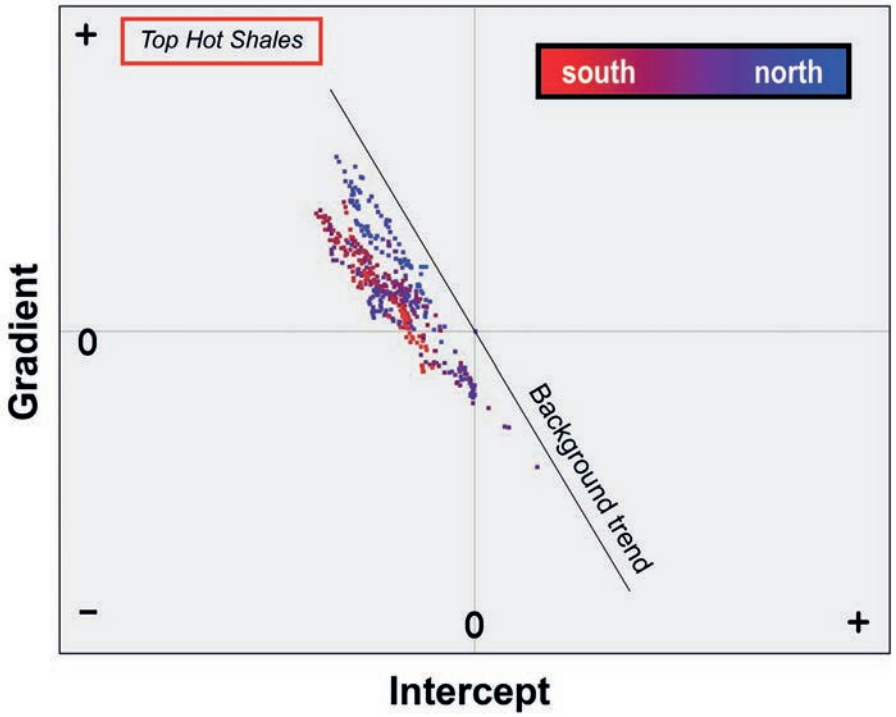

Fig. 9 - Gradient - Intercept AVA plot for the top 'hot shale' interval of the Tanezzuft Fm. The class IV response is evident, and it nearly disappears for data points coming from the northern part of the Ghadames Basin, which is near kerogen lean (modified after Amato del Monte *et al*., 2018).

3.4. Seismic attributes

The sweetness attribute was calculated for the 2D line of the Ghadames Basin, the same used to calculate the model-driven impedance. In Fig. 10 the sweetness image of the line is shown. In Fig. 11 a scatter plot enables comparing the correspondence of sweetness values versus impedance. The data points are extracted at the bottom of the 'hot shale' interval of the Tanezzuft Fm. As can be seen, there is a good correspondence between impedance and sweetness, so the attribute could be used as a substitute for impedance inversion. However, the problem with the sweetness attribute is that it is just a relative indicator of the presence of kerogen. Variations in the source frequency or in the overburden anelastic attenuation would perturb its value, independently of the presence of kerogen.

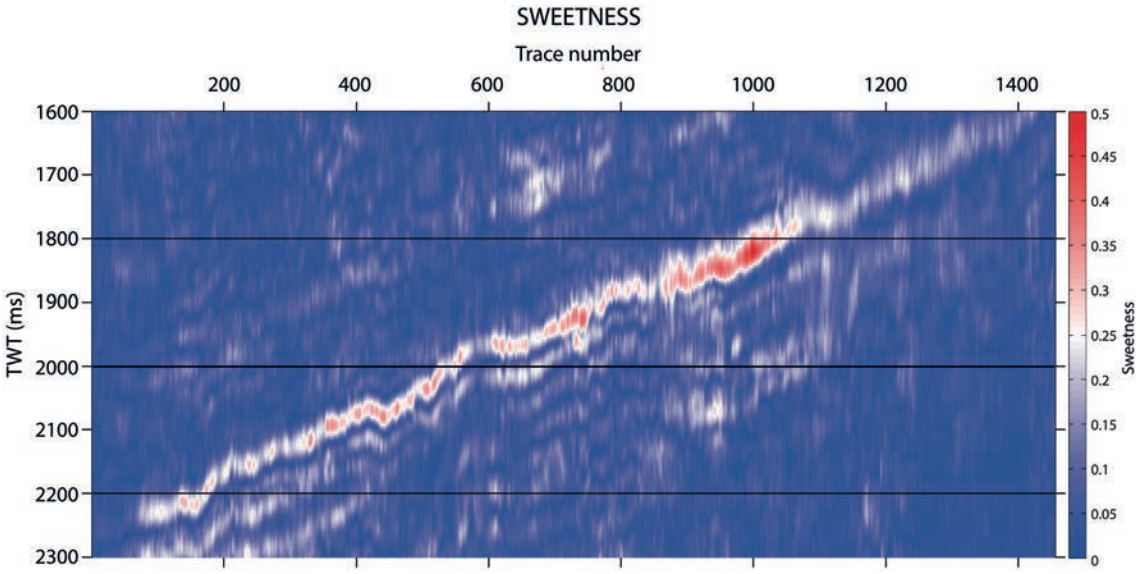

Fig. 10 - Sweetness image of the source rock. The Tanezzuft Fm. is the dipping red event located in the middle of the image.

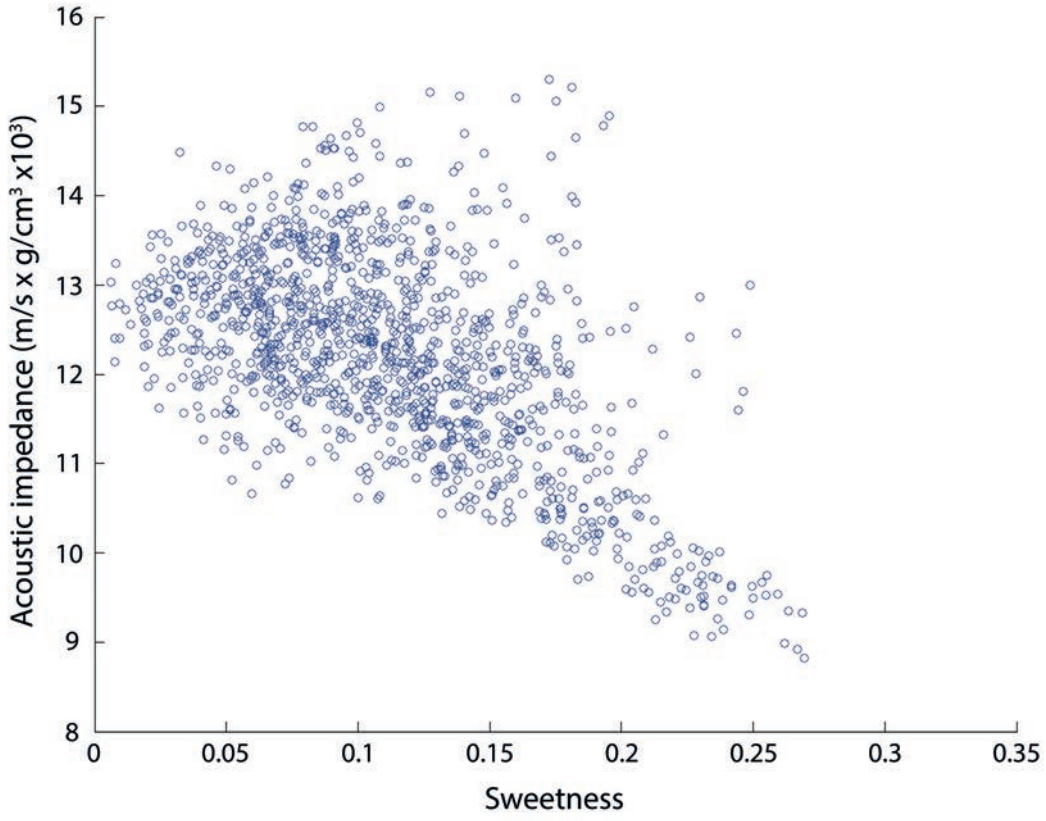

Fig. 11 - Scatter plot of AI - sweetness values for the 'hot shale' formation. As can be seen, AI and sweetness attribute are correlated.

A more meaningful indicator could be a measure of anelastic attenuation but measuring the Q factor from reflection seismic data is not easy. Our attempts to use the instantaneous frequency attribute as a measure of attenuation up to now have proved vexing. In fact, thin layers introduce rapid variations in the instantaneous frequency, and it is difficult to remove them from the main frequency trend.

4. Conclusions

Three methods for qualitative and quantitative kerogen detection have been studied and tested. AI inversion appears to be the most promising method, since, when coupled with a rock physics model, quantitative estimations of *TOC* value can be obtained. Model-based inversion requires an impedance log curve from a nearby well, which is of course missing in newly explored basins. An acoustic inversion method, where the low frequency impedance model is replaced with impedance constraints, has been implemented and tested. Results show that the method could be used in undrilled prospects, however image artifacts result if the quality of the seismic data is not adequate.

AVA analysis can provide useful information on *TOC* distribution, but its application is limited by the availability of log data and possibly core samples. For laminated source rocks, anisotropy should be considered, and in kerogen-rich source rocks the anisotropy could exceed the common small-anisotropy approximation.

A frequency dependent attribute was shown to be qualitatively equivalent to AI inversion. Although it cannot be used to obtain direct measurements of the *TOC* values, it could nevertheless be useful for source rock evaluation in undrilled basins.

The quantitative interpretation of data requires an appropriate rock physics model. The few data available from literature, together with core sample data from the Ghadames Basin, showed that the origin of kerogen (terrestrial versus marine) impacts on its elastic properties, making quantitative measurements of *TOC* ambiguous. The ambiguity can be solved if information about the sedimentary environment is available, so that the expected kerogen type can be estimated. Kerogen anelasticity, although difficult to quantify and potentially adding further uncertainty, offers a way to estimate *TOC* value. However, to date available methods for measuring anelastic attenuation from seismic data are still not sufficient to quantify kerogen presence through its anelasticity. More data are necessary to further our knowledge on kerogen viscoelastic properties and their connection with its origin and maturity.

Acknowledgments. The authors thank Eni management for allowing the publication of this work. We acknowledge the contributions of A. Amato Del Monte, E. Antonielli, G. Luchetti, E. Paparozzi, L. Bianchin, P. Scotti, E. Previde Massara, and A. Ortenzi. The authors also thank the two anonymous referees who helped in improving this work. Part of this paper was presented at the 39th conference of the Italian Group for Solid Earth Geophysics (GNGTS).

REFERENCES

Abdulrazzaq Z.T., Thabit J.M. and Al Khafaji A.J.; 2021: *Performance of GPR attribute analysis to detect and characterise buried archaeological targets near Ukhaidir palace, Iraq*. Boll. Geof. Teor. Appl., 62, 159-172.

Aki K. and Richards P.; 1980: *Quantitative seismology: theory and method*. W.H. Freeman & Co., San Francisco, CA, USA, Vol. I and II, 930 pp., doi: 10.1002/gj.3350160110.

Amato del Monte A., Antonielli E., De Tomasi V., Luchetti G., Paparozzi E. and Gambacorta G.; 2018: *Methods for source rock identification on seismic data: an example from the Tanezzuft Formation (Tunisia).* Mar. Pet. Geol., 91, 108-124.

Bai M.; 2016: *Mechanical characteristics of laminated sand-shale sequences identified from sonic velocity and density correlations.* Geomech. Geophys. Geo-Energy Geo-Resour., 2, 275-300, doi: 10.1007/s40948-016-0036-0.

Barrodale I. and Roberts F.; 1980: *ALGORITHM 552, solution of the constrained l_1 linear approximation problem [F4].* ACM Trans. Math. Software, 6, 231-235,

Bourbié T.; 1982: *Effects of attenuation on reflections*. Ph.D. Thesis in Philosophy, Stanford University, Stanford, CA, USA, 219 pp.

Carcione J.M.; 2000: *A model for seismic velocity and attenuation in petroleum source rocks.* Geophys., 65, 1080-1092.

De Tomasi V.; 2016: *On the estimation of the apparent oscillation frequency of a time series.* In: Proc. SIMAI XIII Biannual Congress, Milano, Italy, pp. 368-372.

Fomel S.; 2007: *Local seismic attributes*. Geophys., 72, A29-A33.

Gambacorta G., Caronni V., Antonielli E., Previde Massara E., Riva A., Scotti P., Trincianti E. and Erba E.; 2016: *Hot shale in an ice world: paleoceanographic evolution of the northern Gondwana margin during the early Paleozoic (Tanezzuft Formation, Tunisia).* Mar. Pet. Geol., 72, 393-411.

Gardner G.H.F., Gardner L.W. and Gregory A.R.; 1974: *Formation velocity and density - the diagnostic basics for stratigraphics traps.* Geophys., 39, 770-780, doi: 10.1190/1.1440465.

Guitton A. and Symes W.W.; 2003: *Robust inversion of seismic data using the Huber norm.* Geophys., 68, 1310-1319.

Kappel F. and Kuntsevich A.V.; 2000: *An implementation of Shor's r-algorithm.* Comput. Optim. Appl., 15, 193-205, doi: 10.1023/A:1008739111712.

Lines L., Wong J., Innanen K., Vasheghani F., Sondergeld C., Treitel S. and Ulrych T.; 2014: *Experimental measurement of Q-contrast reflections.* Geophys. Prospect., 62, 190-195.

Løseth H., Wensaas L., Gading M., Duffaut K. and Springer M.; 2011: *Can hydrocarbon source rocks be identified on seismic data?* Geol., 39, 1167-1170.

Luenberger D.G. and Ye Y.; 2016: *Linear and nonlinear programming, 4th ed*. Springer, Berlin, Germany, 555 pp.

Mavko G., Mukerji T. and Dvorkin J.; 2003: *Rock physics handbook: tools for seismic analysis of porous media.* Cambridge University Press, Cambridge, UK, 523 pp., doi: 10.1017/CBO9780511626753.

Passey Q.R., Creaney S., Kulla J.B., Moretti F.J. and Stroud J.D.; 1990: *A practical model for organic richness from porosity and resistivity logs.* Am. Ass. Pet. Geol. Bull., 74, 1777-1794.

Radovich B.J. and Oliveros R.B.; 1998: *3D sequence interpretation of seismic instantaneous attributes from the Gorgon field*. Leading Edge, 17, 1286-1293.

Rüger A.; 1997: *P wave reflection coefficients for transversely isotropic models with vertical and horizontal axis of symmetry.* Geophys., 62, 713-722.

Shuey R.T.; 1985: *A simplification of the Zoeppritz equations.* Geophys., 50, 609-614.

Taner M.T., Koehler F. and Sheriff R.E.; 1979: *Complex seismic trace analysis.* Geophys., 44, 1041-1063.

Thomsen L.; 1986: *Weak elastic anisotropy.* Geophys., 51, 1954-1966.

Ulrych T.J. and Walker C.; 1984: *On a modified algorithm for the autoregressive recovery of the acoustic impedance.* Geophys., 49, 2190-2192.

Walker C. and Ulrych T.J.; 1983: *Autoregressive recovery of the acoustic impedance.* Geophys., 48, 1338-1350.

Yan F. and Han D.; 2013: *Measurement of elastic properties of kerogen.* In: Proc. SEG 2013 Annual Meeting, Houston, TX, USA, pp. 2778-2782, doi: 10.1190/segam2013-1319.1.

Zezotarsky J., Chromik R.R., Vinci R.P., Messmer M.C., Michels R. and Larsen J.W.; 2004: *Imaging and mechanical property measurements of kerogen via nanoindentation.* Geochim. Cosmochim. Acta, 68, 4113-4119.

Corresponding author: Vittorio De Tomasi
Eni S.p.A. Natural Resources
Via Emilia 1, 20097 San Donato Milanese, Italy
Phone: +39 02 520 62153; e-mail: vittorio.detomasi@eni.